Journal of Statistical Physics, Vol. 56, Nos. 5/6, 1989

Computer Simulation of Driven Diffusive Systems with Exchanges

Jian-Sheng Wang,[1,2] Kurt Binder,[1,3] and Joel L. Lebowitz[1,4]

Received December 9, 1988; final April 25, 1989

The field-driven Kawasaki model with a fraction p admixture of Glauber dynamics is studied by computer simulation: $p=0$ corresponds to the order-parameter-conserving driven diffusive system, while $p=1$ is the equilibrium Ising model. For $p=0.1$ our best estimates of critical exponents based on a system of size 4096×128 are $\beta\approx0.22$, $\eta^{RS}\approx0.45$, and $\nu_{\|}\approx\nu_{\perp}\approx1$. These exponents differ from both the values predicted by a field-theoretic method for $p=0$ and those of the equilibrium Ising model. Anisotropic finite-size scaling analyses are carried out, both for subsystems of the large system and for fully periodic systems. The results of the latter, however, are inconsistent, probably due to the complexity of the size effects. This leaves open the possibility that we are in a crossover regime from $p=0$ to $p\neq0$ and that our critical exponents are "effective ones." For $p=0$ our results are consistent with the predictions $\nu_{\|}>\nu_{\perp}$.

KEY WORDS: Driven Kawasaki models; stochastic lattice gas; nonequilibrium phase transitions; computer simulations; finite-size scaling.

1. INTRODUCTION

Nonequilibrium steady states are still far from being well understood despite considerable study in recent years.[1-10] In the "strongly driven" Kawasaki model in two dimensions, studied extensively in refs. 2, 5, and 9, exchanges of spins (or particle jumps) in the $\pm x$ direction, perpendicular to the field, are made with transition probabililties satisfying the usual detailed balance condition for a nearest neighbor ferromagnetic interaction J,[11] jumps which move particles along the field in the $+z$ direction are

[1] Department of Mathematics, Rutgers University, New Brunswick, New Jersey 08903.
[2] Present address: HLRZ, Kernforschungsanlage Jülich, D-5170 Jülich 1, West Germany.
[3] Permanent address: Institut für Physik, Universität Mainz, D-6500 Mainz, West Germany.
[4] Department of Physics, Rutgers University, New Brunswick, New Jersey 08903.

0022-4715/89/0900-0783$06.00/0

always made, and there are no jumps against the field. The system is thus out of equilibrium, maintaining (via periodic boundary condition) a steady-state current in the $+z$ direction; see ref. 9 for more details.

While the nonequilibrium phase transition of this model is of particular interest,[12,13] its study by computer simulations[3–5,8,9] is difficult for several reasons: (i) There is an extremely pronounced critical slowing down: it is predicted[12,13] that transverse fluctuations relax with a dynamic critical exponent $z_\perp = 4$. (ii) The conservation law makes it difficult to obtain the order parameter and susceptibility (see Appendices A and B). (iii) There are complicated finite-size effects.

The first two difficulties are avoided if we consider a modified model where, in addition to the exchanges according to the rules summarized above, one also allows for spin flips to occur a fraction p of the time, according to a Glauber flip rate.[14,15] This destroys the conservation law of the magnetization: now both the order parameter $\langle |\mathcal{P}| \rangle$ and susceptibility χ can be straightforwardly sampled. Even for p as small as 0.1 the relaxation toward the steady state is distinctly faster than for the strictly conserved case ($p = 0$). This model for $p < 1$ still exhibits a steady-state current, and thus its phase transition should belong to a class of nonequilibrium phase transitions, although presumably with exponents different from those of the driven Kawasaki model and also from those of the standard Ising model equilibrium phase transition. Unfortunately, we pay for the computational advantages of this model with disadvantages: (i) Unlike the standard driven Kawasaki model,[12,13] there are no field-theoretic predictions available for this model. (ii) Since for $p \to 0$ a crossover to the driven Kawasaki model and for $p \to 1$ a crossover to the standard equilibrium Ising model must occur, the critical region where the asymptotic behavior for values of p in between these limits occurs might be rather narrow. If for small p the critical behavior of the driven Kawasaki model is the same as for $p = 0$, it would serve our purpose; but if it were already dominated by the Ising critical behavior, no information would be gained about nonequilibrium steady states at $p = 0$.

In the following sections, we report results of extensive computer simulations at $p = 0.1$ and also some results at $p = 0$ and $p = 0.5$. A discussion is given at the end.

2. DRIVEN KAWASAKI MODEL WITH $p = 0.1$

2.1. Order Parameter

We carried out simulations of the modified driven Kawasaki model with $p = 0.1$ on square lattices with sizes 8×8, 16×16, 32×32, 64×64, and

128×128. The updating of system states is typically 10^5 Monte Carlo steps per spin, with the first 10^4 steps discarded in a run, unless starting from a previous stationary state configuration.

The modified dynamics enables us to calculate order parameters by computing the absolute value of the total magnetization or the square root of the second moment of the magnetization. The difference between the two is small [it is approximately $\chi/(2mN)$, where χ is the susceptibility and N is the size of the system], but the latter is numerically more accurate. By observing this, we find that the system orders at a temperature T_c. We also noticed metastability problems for large systems when $T < T_c$: once a domain wall (strip configuration) is formed,[5] it is very difficult to remove. So we always started with a configuration whose total magnetization is approximately the stationary state magnetization.

Figure 1 is a plot of $m \equiv \langle \Psi^2 \rangle^{1/2}$ vs. $K = J/k_B T$ for various sizes. We see clearly an L^{-1} size dependence at high temperatures. This is similar to

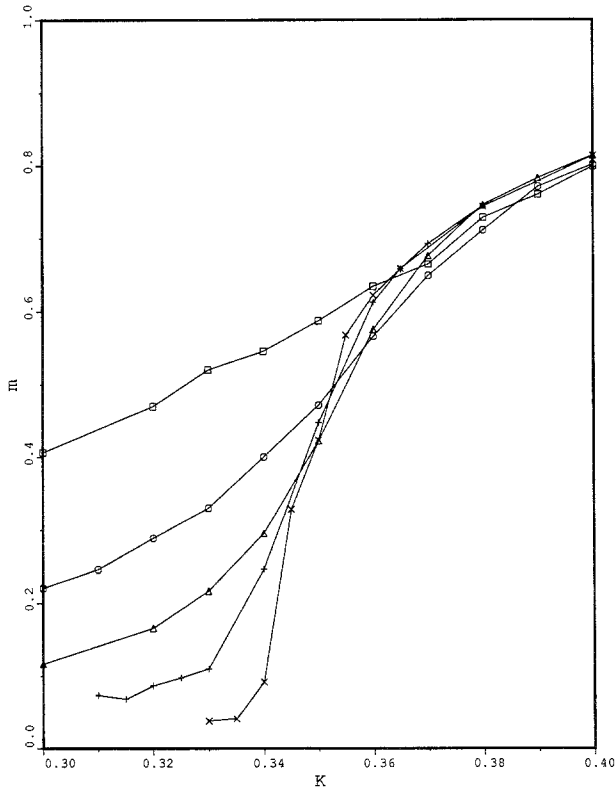

Fig. 1. Mean-root-square magnetization m vs. dimensionless inverse temperature $K = J/k_B T$ for sizes (□) 8×8, (○) 16×16, (△) 32×32, (+) 64×64, (×) 128×128.

equilibrium behavior and indicates an approximate independent distribution for blocks of spins with linear dimensions larger than the correlation length. At low temperatures finite-size effects are small and the order parameter appears to converge to its infinite-volume limit very fast. This is in contrast to the result of Vallés and Marro (ref. 5, Fig. 5a) for $p=0$, where the order parameter, defined in a different way (see Appendix B), shows large finite-size effects both above and below the transition temperature. The low-temperature finite-size effects in their model are clearly due to the conservative nature of the dynamics at $p=0$. Near the phase transition the finite-size effect is complicated also for $p\neq 0$ due to anisotropy. Finite-size scaling analysis will be presented in later subsections.

Figure 2 is a plot of $m^{1/\beta}$ vs. K for a system of size 128×128, taking for β the mean-field value 1/2, the two-dimensional Ising value 1/8, and the

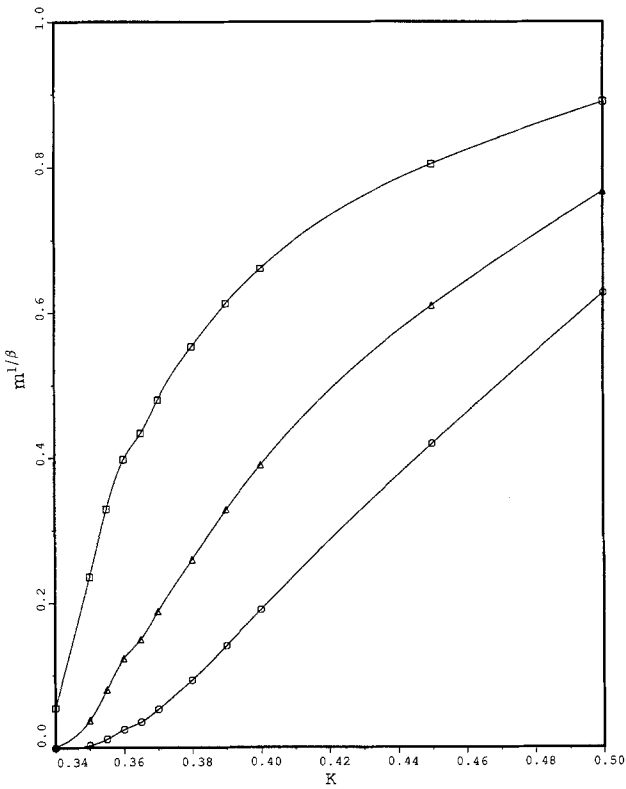

Fig. 2. $m^{1/\beta}$vs. K for different values of β. The top curve corresponds to $\beta=1/2$; the bottom curve to $\beta=1/8$; the middle one to $\beta=0.22$. The data are from a 128×128 system.

empirical value 0.22, respectively. We see from the plot that for $K > 0.4$ the curve for $\beta = 1/8$ becomes a straight line. This might have something to do with crossover to Ising behavior. For $K < 0.36$ the data are not very reliable due to finite-size effects. Relying on the data between 0.36 and 0.40, we perform a least-square fit to a form

$$m = a|K - K_c|^{\beta}. \tag{1}$$

Such a fit leads to $K_c = 0.343 \pm 0.003$ and $\beta = 0.22 \pm 0.02$ (see also next section for different ways of finding T_c). Our result should be compared with $\beta = 0.230 \pm 0.003$ at $p = 0$ of Vallés and Marro.[5] We cannot rule out the possibility that m behaves differently very close to T_c.

2.2. Correlation Functions

We studied the pair correlation functions $G_{\perp}(x) = \langle \Psi(0, 0)\, \Psi(x, 0) \rangle$ and $G_{||}(z) = \langle \Psi(0, 0)\, \Psi(0, z) \rangle$ for a square with linear dimension

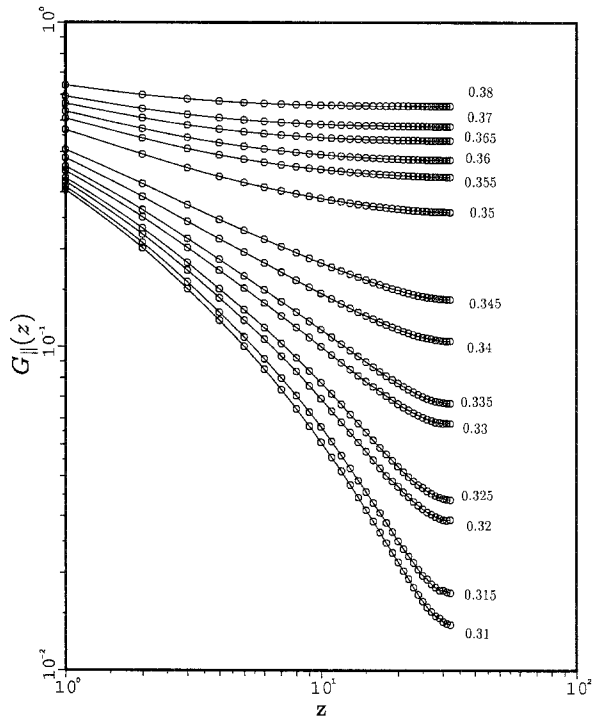

Fig. 3. Longitudinal two-point correlation function plotted in log–log scale for system of size 64×64. Note that due to the periodic boundary conditions $G_{||}(z) = G_{||}(L_{\max} - z)$ and thus only distances $z < L_{\max}/2$ have been included. Various inverse temperatures are shown, as indicated in the figure.

$L_{\max} = 64$ (see Figs. 3 and 4). One can see that both types of correlations indicate that the system is ordered for $K \geqslant 0.35$ and disordered for $K \leqslant 0.34$. To obtain more quantitative results about T_c and various critical exponents we need to minimize the finite-size effect. Knowing that the system can be highly anisotropic, we investigated a large system of size 4096×128. To locate T_c accurately, we performed simulation at $K = 0.343$, 0.342, 0.341, and so on. Figures 5 and 6 show longitudinal and transverse correlation functions on log–log plots. From the plots we see that K_c is somewhere between 0.341 and 0.343, consistent with the previous results on smaller systems.

To our surprise, the slopes of the straight lines for both longitudinal and transverse correlations at K closest to K_c give exponents $\eta_{\|}^{\mathrm{RS}} \approx \eta_{\perp}^{\mathrm{RS}} = 0.45 \pm 0.05$. For comparison, the field-theoretic results for $p = 0$ are $\eta_{\|}^{\mathrm{RS}} = 2/3$, $\eta_{\perp}^{\mathrm{RS}} = 2$,[12,13] while the $p = 1$ standard Ising model value is $\eta = 1/4$. It is very convincing that $\eta_{\|}^{\mathrm{RS}} \approx 0.45$. The power-law decay is displayed in a range from $z = 4$ to 100 [the distance z can actually start from

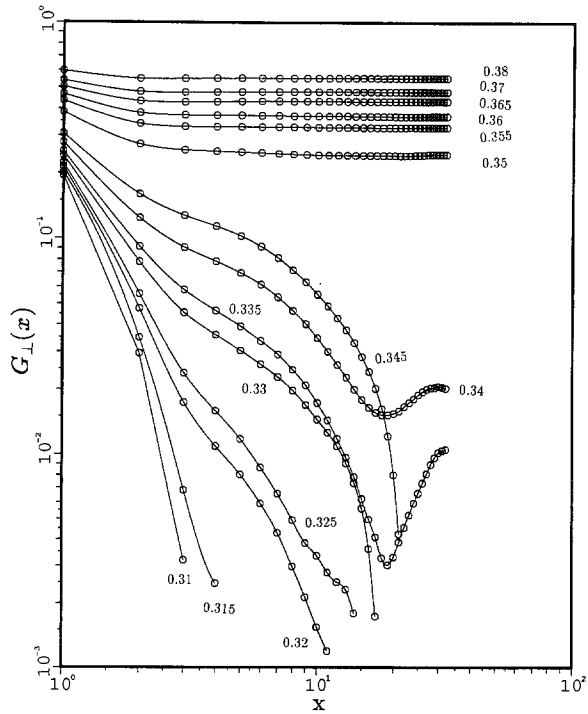

Fig. 4. Transverse correlation function plotted in log–log scale for a system of size 64×64. Note the difference in coordinate scales as compared to Fig. 3.

1, but we measured $G_{||}(z)$ only at z a multiple of 4; see Fig. 3]. On the other hand, the power-law behavior for the transverse correlation function is in a narrow range, from $x=3$ to 13, and the initial decay ($x \leqslant 2$) of the transverse correlation is very fast and does not follow the long-distance power law. At very large distances both transverse and longitudinal correlation functions tend to the same nonzero constants, which depend on temperature and are somewhat different from run to run. This, we think, is due to the fact that $\langle \Psi^2 \rangle$ is nonzero even at T_c for finite systems and/or to the system not being in a stationary state at large scales.

We note that although the exponents $\eta_{||}^{RS}$ and $\eta_{\perp}^{RS}$ seem to be the same, the amplitudes of the power-law decays are quite different. The effect of anisotropy is thus reflected in the amplitudes only, if this interpretation of the data is correct. In fact, the correlation functions can be described at T_c by $G_{\perp}(x) \approx 0.16x^{-\eta}$, $G_{||}(z) \approx 0.15(z/10)^{-\eta}$ with $\eta = 0.45$. This suggests that $p=0.1$ is the right scaling factor for the field direction.

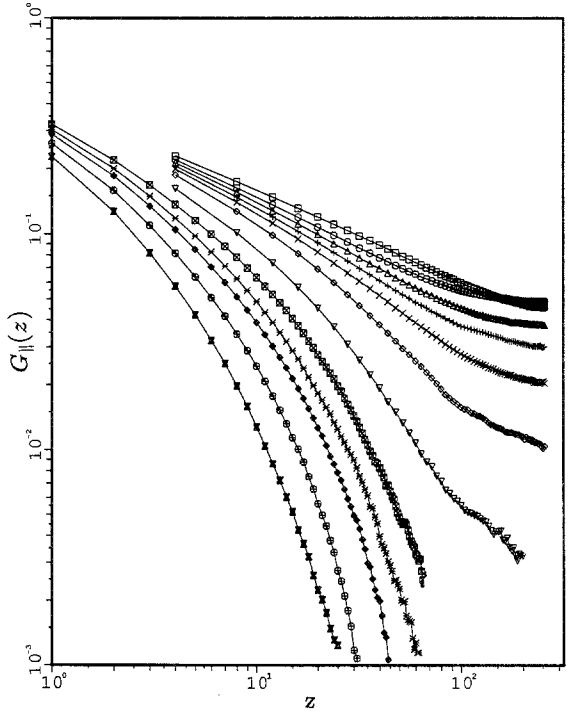

Fig. 5. Longitudinal correlation functions plotted in log–log scale for a system of size 4096×128 at dimensionless inverse temperature $K = J/k_B T = 0.343$, 0.342, 0.341, 0.340, 0.339, 0.337, 0.33, 0.32, 0.31, 0.30, 0.28, and 0.25, from top to bottom, respectively.

Figures 7a and 8a are semilog plots of longitudinal and transverse correlation functions. There are fast, nonexponential, decays at short distances. The correlation functions appear nonexponential even at large distances except at very high temperatures, where the system has to have exponential decay behavior whenever $p \neq 0$. (For $p = 0$, the correlation function behaves like r^{-2} at high temperature.[9]) Normalizing the correlation function by the critical power law gives better exponential behavior, as can be seen by comparing Fig. 7a and Fig. 7b or Fig. 8a and Fig. 8b, where in Fig. 7b $G_{||}(z)$ is multiplied by $z^{0.45}$, and in Fig. 8b $G_{\perp}(x)$ is multiplied by $x^{0.44}$. The correlation lengths $\xi_{||}$ and $\xi_{\perp}$ extracted from the slope of the straight lines in these figures are plotted in Fig. 9 vs. $(K_c - K)/K_c$ on a log–log scale. This analysis gives $\nu_{||} \approx \nu_{\perp} \approx 1.07$. Although it appears that $\nu_{\perp} \approx \nu_{||}$, the correlation length $\xi_{\perp}$ is, as mentioned before, only $0.1\xi_{||}$. In Fig. 10 we plot $z^{\eta_{||}^{RS}} G_{||}$ vs. scaled variable $z/\xi_{||}$ on a log–log scale. The data scale very well. Figure 11 is a similar plot for the transverse correlation function. By comparison with the longitudinal case, the quality of the data

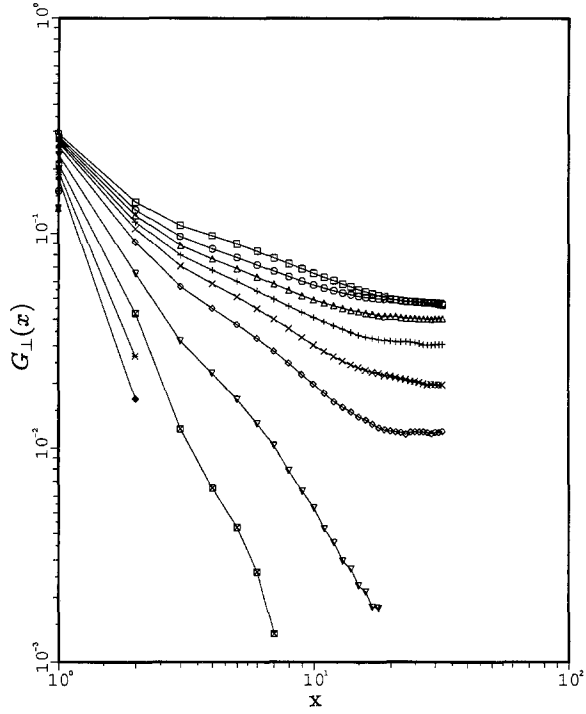

Fig. 6. Transverse correlation functions plotted in log–log scale for a system of size 4096×128 at same the K's as in Fig. 5.

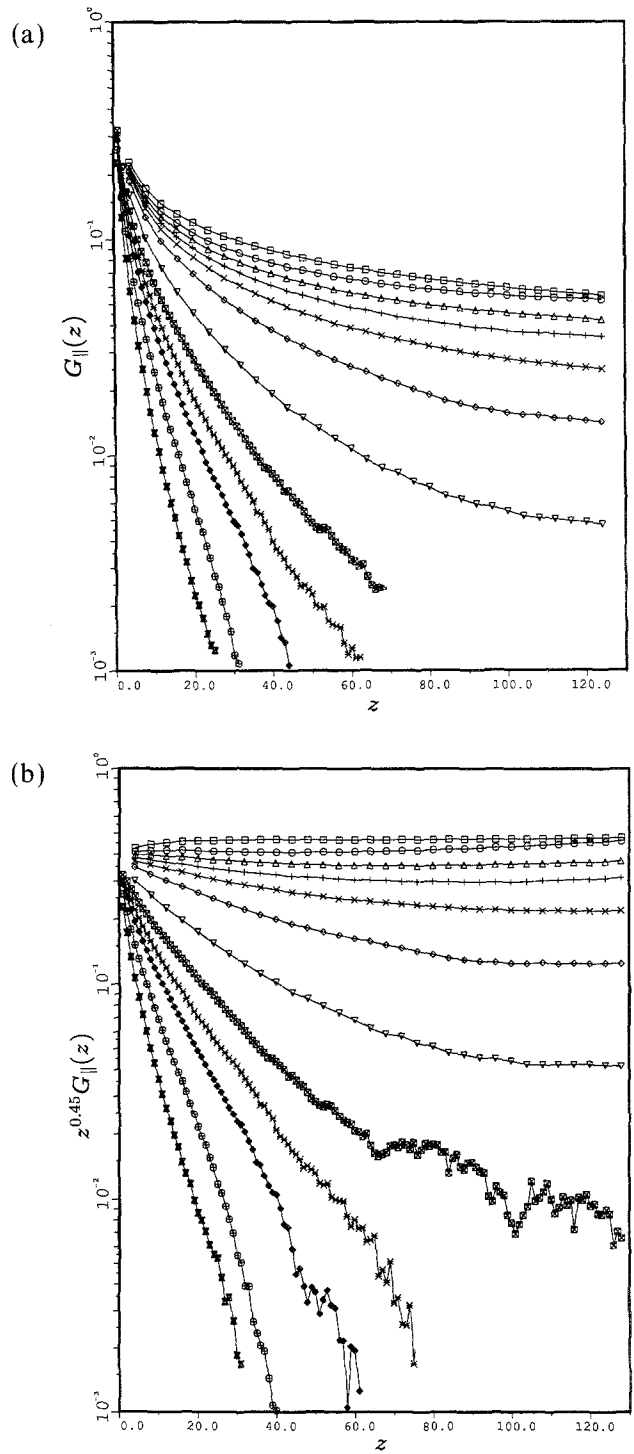

Fig. 7. (a) Longitudinal correlation functions plotted in semilog scale for a system of size 1024×128 at same the K's as in Fig. 5. (b) Same as (a), except that $G_{\|}$ is multipled by $z^{0.45}$.

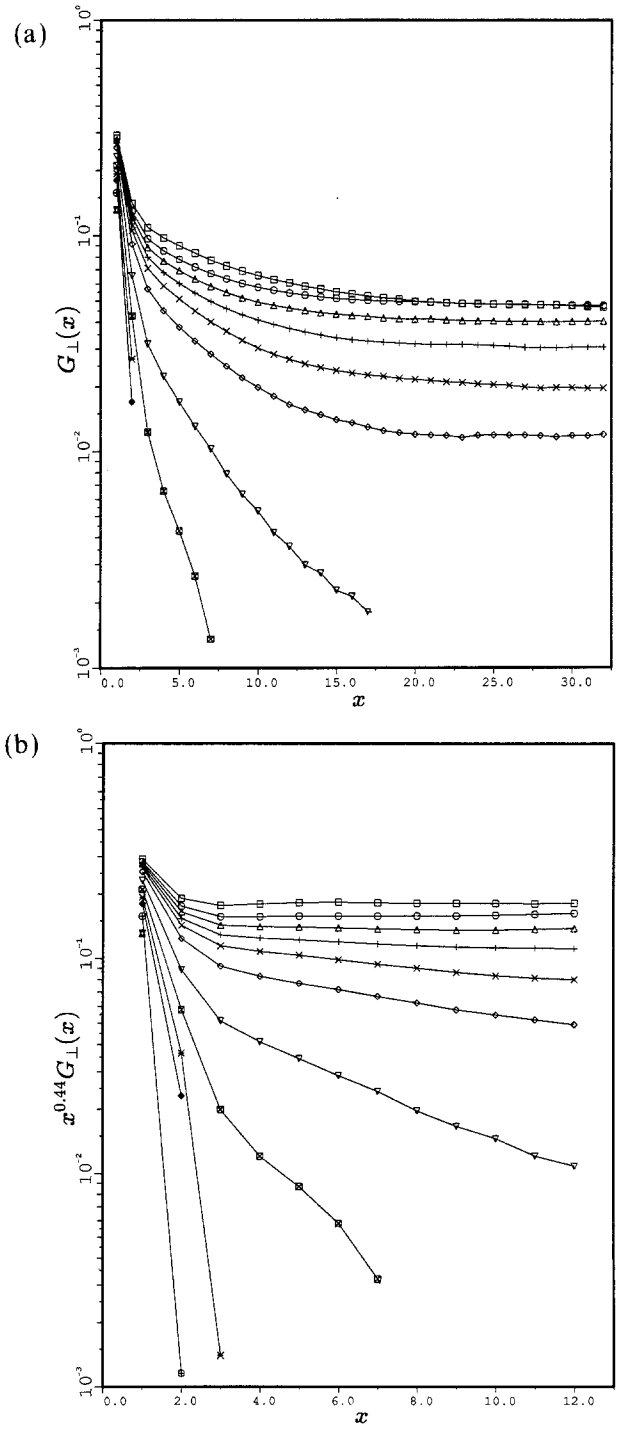

Fig. 8. (a) Transverse correlation functions plotted in semilog scale for system of size 1024×128 at the same K's as in Fig. 5. (b) Same as (a), except that $G_\perp$ is multipled by $x^{0.44}$.

is much worse. We omitted data points at $x = 1$, which clearly do not obey scaling.

In summary, this analysis of correlation functions supports isotropic exponents with anisotropic amplitudes. For a system with isotropic exponents in dimension $d = 2$, the scaling relations $\gamma + 2\beta = d\nu$ and $\gamma = (2 - \eta)\nu$ imply $\nu = 2\beta/\eta$. Using $\beta \approx 0.22$ and $\eta \approx 0.45$, this would yield $\nu \approx 1$, consistent with the above direct analysis.

2.3. Subsystem Scaling

The direct analysis of the data presented in the previous section may be tainted by crossover effects. The quoted numbers for exponents may simply be "effective exponents," not characteristic of the true critical behavior. We therefore now apply the finite-size scaling theory for subsystems with anisotropic critical exponents developed in ref. 16. Unlike

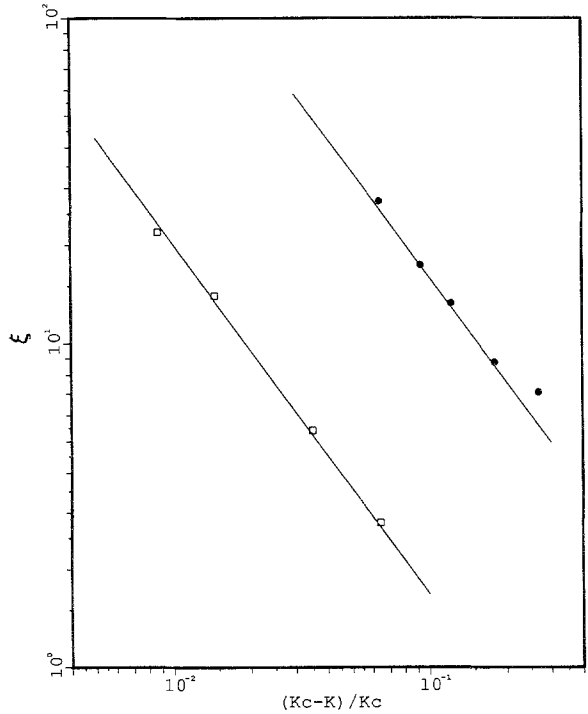

Fig. 9. Longitudinal correlation length $\xi_{\|}$ (solid circles) and transverse correlation length $\xi_{\perp}$ (squares) vs. reduced temperature $t = (K_c - K)/K_c$ in log–log scale. Correlation lengths are extracted from Figs. 7b and 8b. The straight lines are given by $\xi_{\|} = 1.37t^{-1.07}$, $\xi_{\perp} = 0.14t^{-1.08}$.

finite-size scaling for isotropic systems, two lengths (longitudinal and transverse) have to be considered in the analysis.

The advantage of considering subsystems of a large system (4096×128) is that data on various combinations of sizes can be obtained in a single run, while for fully periodic finite systems each size has to be simulated independently. The disadvantages are that "equilibration" of the whole system is difficult and finite-size effects due to finiteness of the large system occur and are not well understood. We discuss here the results of subsystem scaling. Fully periodic finite systems are presented later.

A useful way to check the location of T_c when different sizes are available is to look at the reduced fourth moment of the magnetization $g = (3 - \langle \Psi^4 \rangle / \langle \Psi^2 \rangle^2)/2$ for different subsystems. In Fig. 12a and 12b we plot g vs. K for sizes $L_{||} = L_\perp$ and $L_{||} = L_\perp^2$. The intersections give estimates for K_c. By comparing with runs on smaller lattices, we notice that a subsystem of size 32×32 already feels the finiteness of the whole system. If we consider only data from sizes 4×4, 8×8, 16×16, 16×4, and 64×8, the value

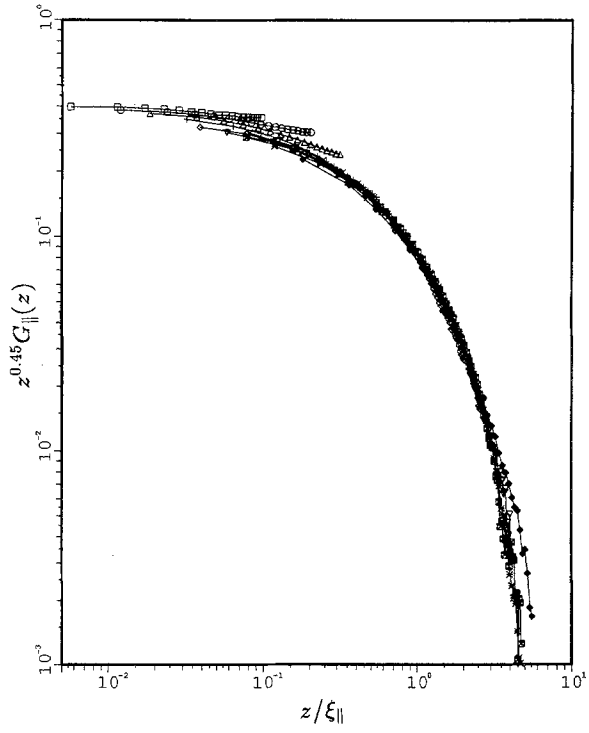

Fig. 10. Scaling plot $z^{0.45}G_{||}(z)$ vs. $z/\xi_{||}$.

K_c is in the range 0.341–0.344. This is consistent with our previous estimates from other data.

The behavior of the size dependence would be simpler if one of the dimensions of the system is much larger than the other. More precisely, the susceptibility and magnetization at K_c are given by[16]

$$\chi \propto L_{||} L_{\perp}^{\gamma/\nu_\perp - \nu_{||}/\nu_\perp}, \quad \langle |\Psi| \rangle \propto L_{\perp}^{-\beta/\nu_\perp}, \quad L_{||} \ll L_{\perp}^{\nu_{||}/\nu_\perp} \tag{2}$$

$$\chi \propto L_{\perp} L_{||}^{\gamma/\nu_{||} - \nu_\perp/\nu_{||}}, \quad \langle |\Psi| \rangle \propto L_{||}^{-\beta/\nu_{||}}, \quad L_{||} \gg L_{\perp}^{\nu_{||}/\nu_\perp} \tag{3}$$

Figure 13 is a plot of the subsystem susceptibility against $L_\perp$ for different $L_{||}$, plotted on a $\log_2$–$\log_2$ scale. Figure 14 is a similar plot for the magnetization. The limiting behavior, $L_{||} \ll L_{\perp}^{\nu_{||}/\nu_\perp}$, is achieved relatively easily. From this limit we have

$$\gamma/\nu_\perp - \nu_{||}/\nu_\perp = 0.56 \pm 0.06, \qquad \beta/\nu_\perp = 0.23 \pm 0.03 \tag{4}$$

The errors are estimated from the error in K_c and from the fact that Eq. (2) is only *approximately* obeyed; the exponents depend slightly on the shorter

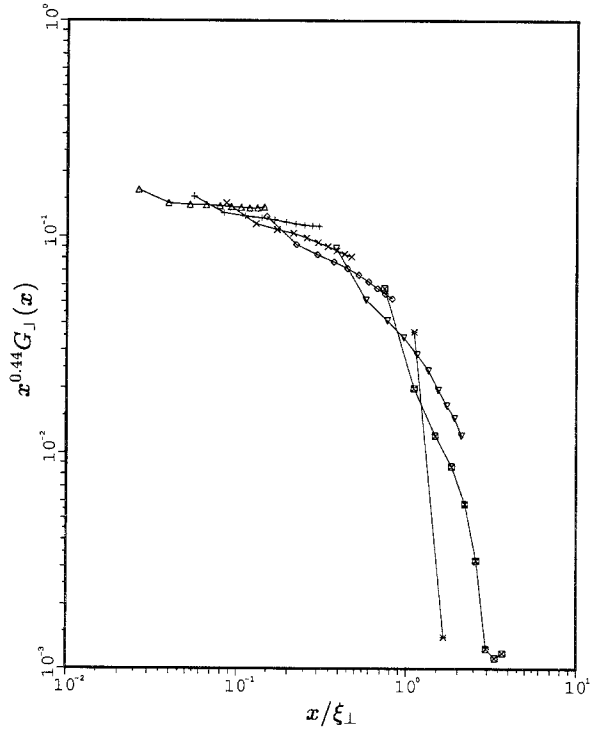

Fig. 11. Scaling plot $x^{0.44}G_\perp(x)$ vs. $x/\xi_\perp$.

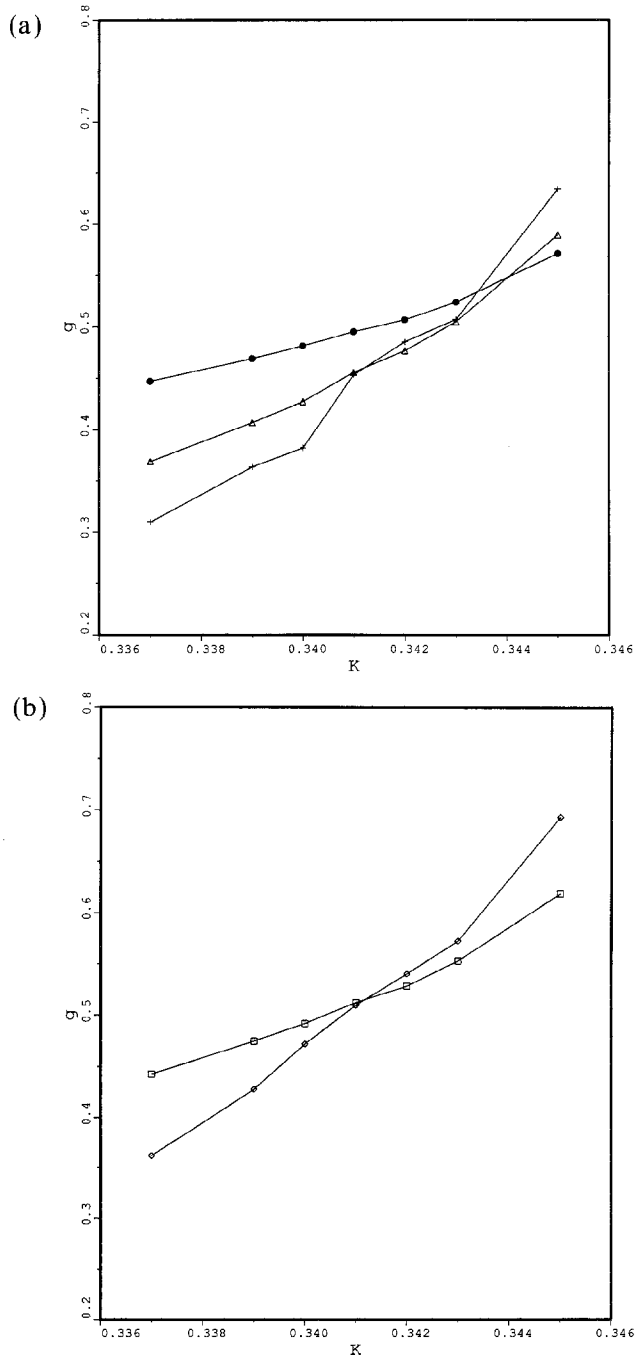

Fig. 12. The fourth moments g of subsystems from a system of size 4096×128 vs. K. (a) Subsystems with $L_{||} = L_{\perp}$. (●) $L_{\perp} = 4$, (△) $L_{\perp} = 8$, (+) $L_{\perp} = 16$. (b) Subsystems with $L_{||} = L_{\perp}^2$. (□) $L_{\perp} = 4$, (◇) $L_{\perp} = 8$.

dimension [$L_{||}$ in Eq. (2)] also. These exponents satisfy well the hyperscaling relation $2\beta/\nu_\perp + \gamma/\nu_\perp = 1 + \nu_{||}/\nu_\perp$. The other limit, $L_{||} \gg L_\perp^{\nu_{||}/\nu_\perp}$, seems difficult to reach. We find, with large error bars, $\gamma/\nu_{||} - \nu_\perp/\nu_{||} = 0.6 \pm 0.1$. Using the hyperscaling relations $\gamma = \nu_{||} + \nu_\perp - \nu_{||}\eta_{||}^{RS}$ and $\nu_{||}\eta_{||}^{RS} = \nu_\perp \eta_\perp^{RS}$, the results given in (4) imply $\eta_\perp^{RS} = 1 - (\gamma/\nu_\perp - \nu_{||}/\nu_\perp) = 2\beta/\nu_\perp = 0.44$–$0.46$, which is consistent with direct evaluation. Results in (4) are thus consistent with $\nu_{||} \approx \nu_\perp \approx 1$, $\eta_{||}^{RS} \approx \eta_\perp^{RS} \approx 0.45$, $\beta \approx 0.22$, and $\gamma \approx 1.55$.

Next we consider the full scaling behavior of the subsystem susceptibility and magnetization. If we take $\nu_\perp/\nu_{||}$ and $\gamma/\nu_{||}$ (or $\beta/\nu_{||}$ for the magnetization) as two free parameters, many values can give apparently "good" scaling plots. The data seem most consistent with $\nu_\perp/\nu_{||}$ being close to 1. They are thus is accordance with results in the previous subsection, $\eta_{||}^{RS} \approx \eta_\perp^{RS}$, if the scaling relation $\nu_{||}\eta_{||}^{RS} = \nu_\perp \eta_\perp^{RS}$ is invoked. Figures 15 and 16 show data collapsing using the following choice of exponent ratios:

$$\nu_\perp/\nu_{||} = 1.0, \qquad \beta/\nu_{||} = 0.22, \qquad \gamma/\nu_{||} = 1.55 \tag{5}$$

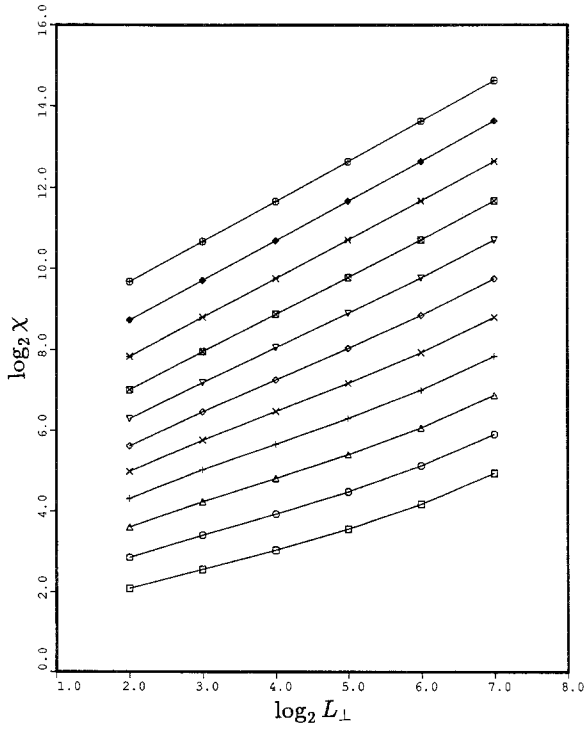

Fig. 13. Subsystem susceptibility plotted against $L_\perp$ for given $L_{||}$ at $K = 0.342$. The curves are guides for the eye. From bottom up: $L_{||} = 4, 8, 16, 32, \ldots, 4096$.

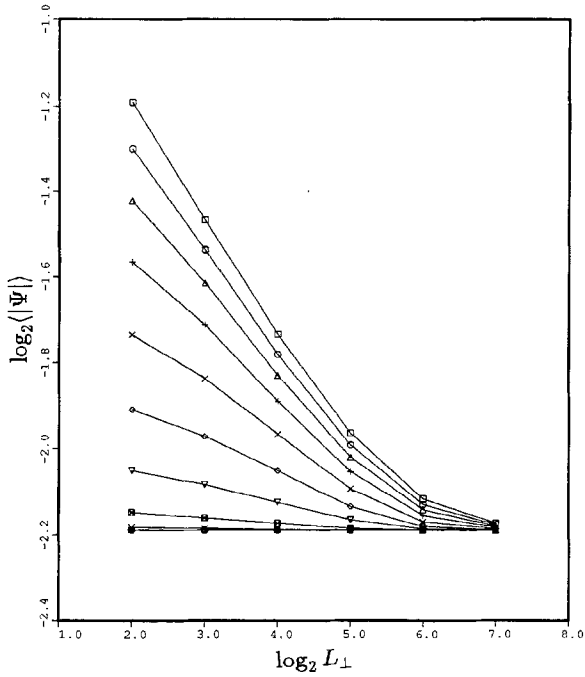

Fig. 14. Subsystem magnetization plotted against $L_\perp$ for given $L_{||}$ at $K=0.342$. The curves are guides for the eye. From top down: $L_{||}=4$, 8, 16, 32,..., 4096.

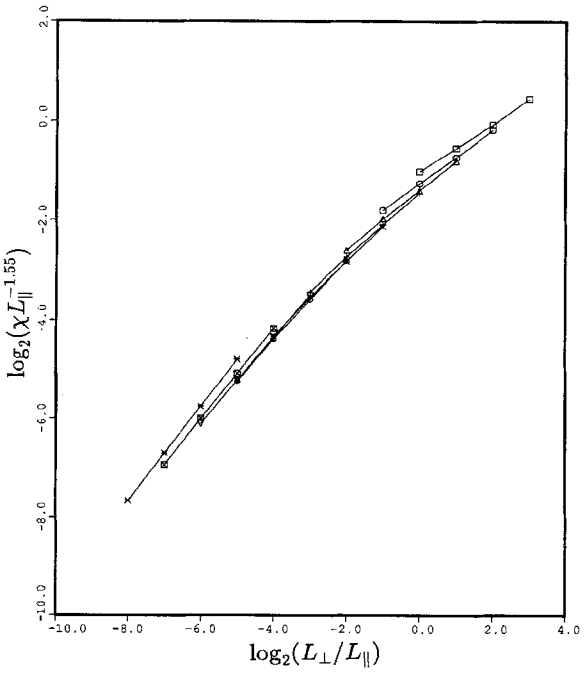

Fig. 15. Subsystem scaling plot $\chi L_{||}^{-\gamma/\nu_{||}}$ vs. $L_\perp/L_{||}^{\nu_\perp/\nu_{||}}$, with $\gamma/\nu_{||}=1.55$, $\nu_\perp/\nu_{||}=1$, taking subsystems of size up to 1024×32.

Figure 17 is a plot of the reduced fourth moment against $L_\perp/L_\parallel$ for each $L_\parallel$. We notice that the peak formed by the envelope of curves occurs at $L_\parallel/L_\perp \approx 10$, indicating that the system is most ordered in such a geometry. These scaling plots should be compared with similar plots for the Ising model.[16]

2.4. Scaling of Fully Periodic Systems

2.4.1. Systems with Sizes $L_\parallel = L_\perp^n$. We also carried out a finite-size scaling analysis with fully periodic blocks, choosing $L_\perp = 3, 4, 5, 6$ and $L_\parallel = L_\perp^3$, as well as $L_\perp = 4, 6, 8, 10, 14$ and $L_\parallel = L_\perp^2$, thus choosing integer exponents $n = 2, 3, 4$ in the relation $L_\parallel = L_\perp^n$. Finally, the cases $L_\perp = 3, 4, 5$ and $L_\parallel = L_\perp^4$, and $L_\perp = 4, 8, 16$ and $L_\parallel = L_\perp$ were also treated. We now expect that in a plot of g vs. K a unique intersection point will occur for $L_\parallel \sim L_\perp^{\nu_\parallel/\nu_\perp}$. This property is tested in Fig. 18. It is seen that for $L_\parallel = L_\perp$ the g vs. K curves for different linear dimensions have no intersection anywhere

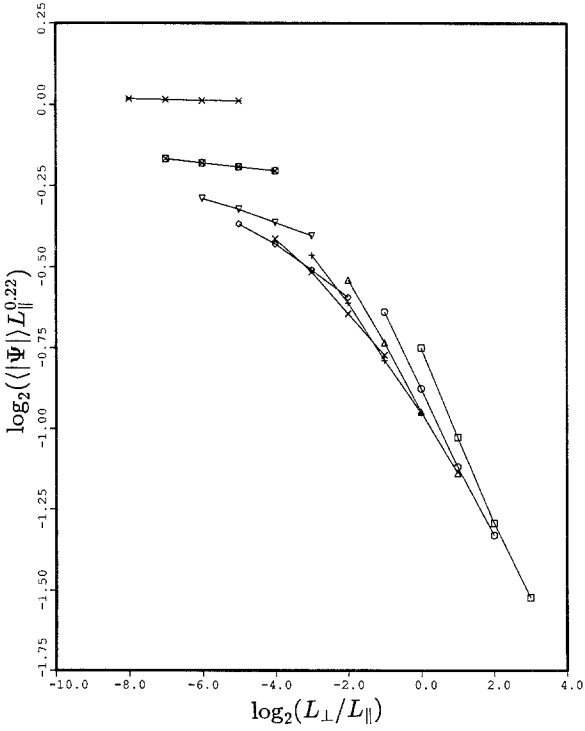

Fig. 16. Subsystem scaling plot $\langle|\Psi|\rangle L_\parallel^{\beta/\nu_\parallel}$ vs. $L_\perp/L_\parallel^{\nu_\perp/\nu_\parallel}$. Here $\beta/\nu_\parallel = 0.22$, $\nu_\perp/\nu_\parallel = 1$, taking subsystems of size up to 1024×32.

in the temperature region where T_c should occur (i.e., in between $K = 0.33$ and 0.35). The curves intersect at much too low a temperature ($K = 0.36$). For $L_{||} = L_{\perp}^2$, on the other hand, intersection points are found for $K = 0.34$–0.35. These values of K are comparable with other estimates of the critical temperature. For $L_{||} = L_{\perp}^3$ and $L_{\perp}^4$ the intersections occur again at lower temperatures ($K = 0.35$ and 0.36, respectively). This behavior of g is quite different from its behavior in subsystems (Fig. 12) where good intersection points occur. The corresponding temperature is insensitive to the choice of $v_{||}/v_{\perp}$ and is in the range of the correct T_c. This difficulty of the fully periodic systems could be caused by the high anisotropy in the amplitudes of singular quantities. If $v_{||} = v_{\perp}$ is true, the system will look isotropic if the longitudinal distance is shrunk by a factor of 10. That means a uniformly ordered system at low temperature is a system for which $L_{\perp} \approx L_{||}/10$. The fourth moments of such systems should intersect at a unique point. On the other hand, the behavior of g for fully periodic systems suggests that $v_{||}/v_{\perp}$ is close to 2 or 3.

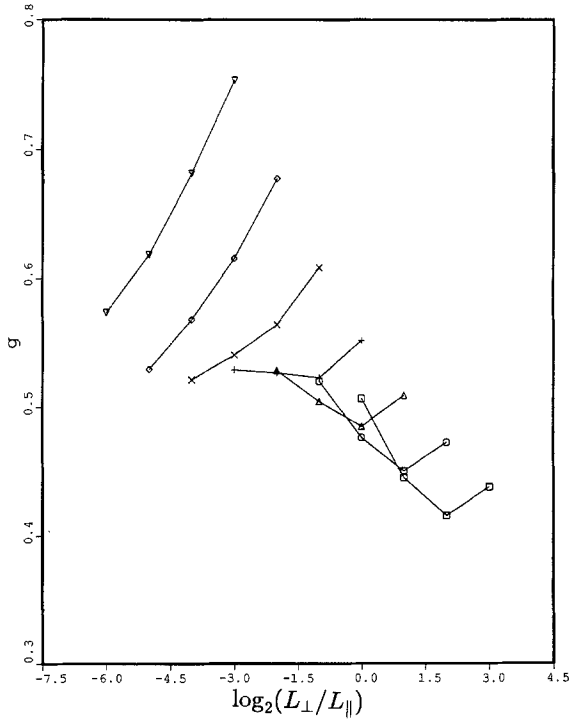

Fig. 17. Subsystem fourth moments g vs. $L_{\perp}/L_{||}$, taking subsystems of size up to 256×32. From bottom up, $L_{||} = 4, 8, 16, \ldots, 256$.

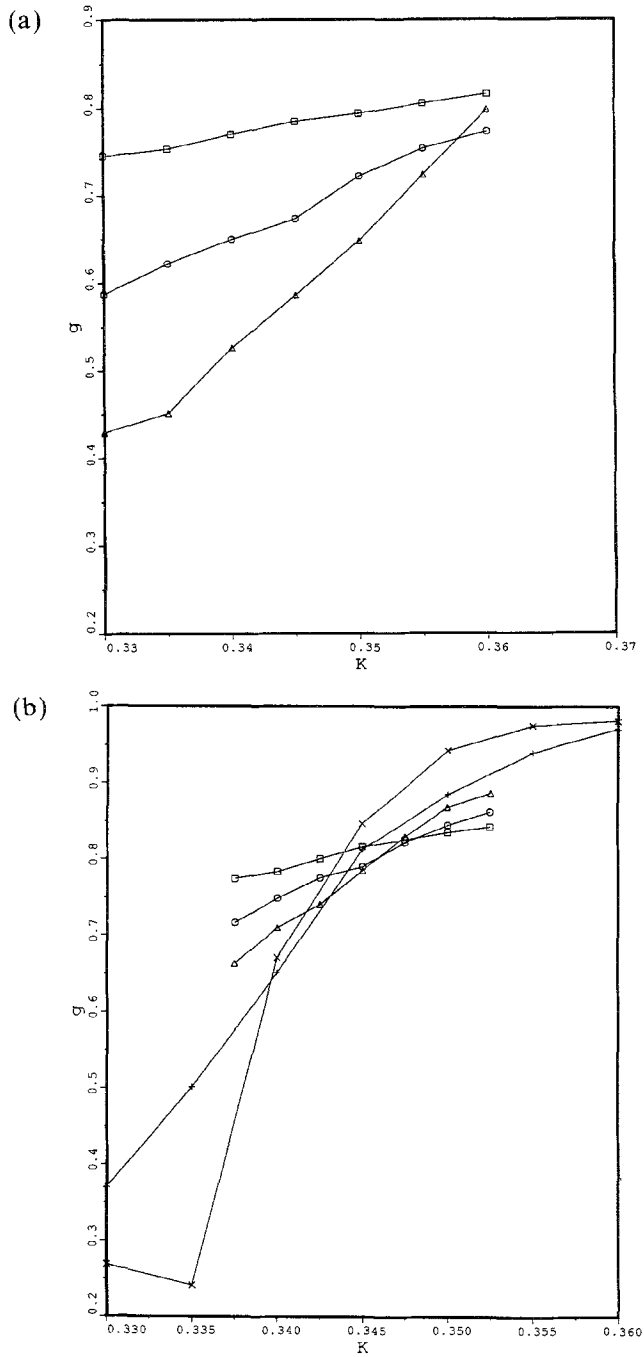

Fig. 18. Fourth moments of fully finite systems for different $L_{||}$ and $L_{\perp}$ relations. (a) $L_{||} = L_{\perp}$, (□) $L_{\perp} = 4$, (○) $L_{\perp} = 8$, (△) $L_{\perp} = 16$; (b) $L_{||} = L_{\perp}^2$, (□) $L_{\perp} = 4$, (○) $L_{\perp} = 6$, (△) $L_{\perp} = 8$, (+) $L_{\perp} = 10$, (×) $L_{\perp} = 16$; (c) $L_{||} = L_{\perp}^3$, (□) $L_{\perp} = 3$, (○) $L_{\perp} = 4$, (△) $L_{\perp} = 5$, (+) $L_{\perp} = 6$, (×) $L_{\perp} = 7$; (d) $L_{||} = L_{\perp}^4$, (□) $L_{\perp} = 3$, (○) $L_{\perp} = 4$, (△) $L_{\perp} = 5$.

(c)

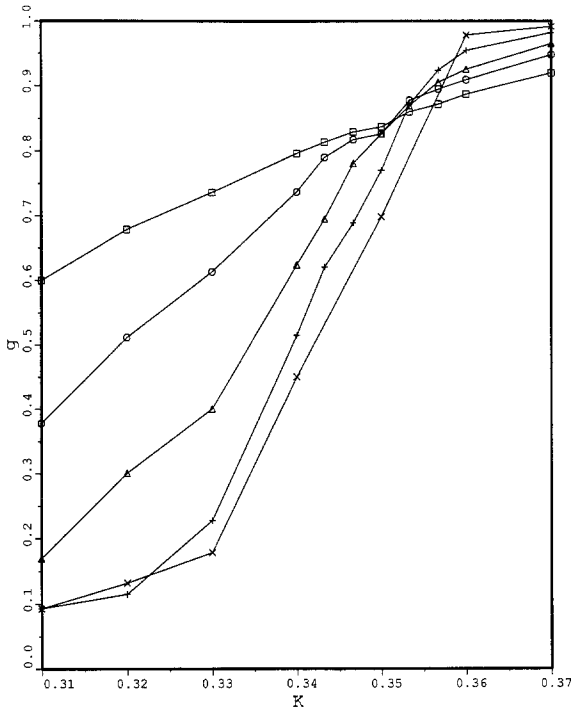

(d)

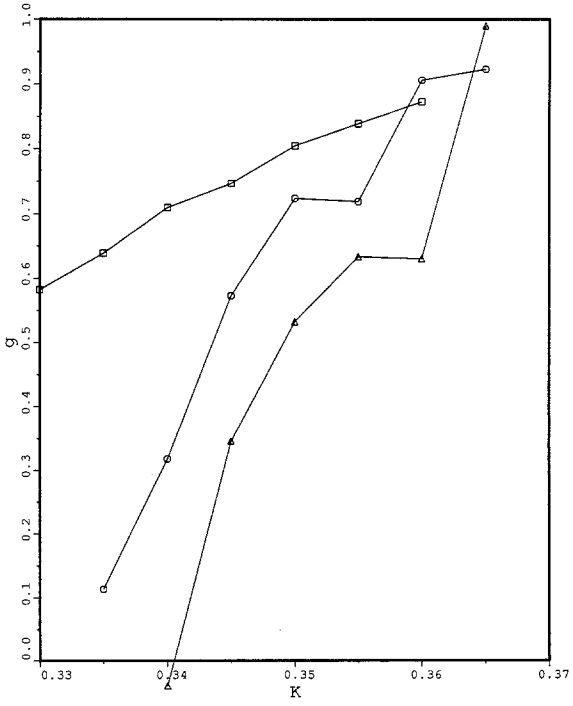

Fig. 18 (*continued*)

Table I. Effective Exponents from Scaling of Finite Periodic Systems at $K_c \approx 0.342$

n	$\beta/\nu_{\|\|}$	$\gamma/\nu_{\|\|}$	$\nu_\perp/\nu_{\|\|}$	$\nu_\perp/\nu_{\|\|} - 1/n$
1	0.43	1.32	1.18	0.18
2	0.26	1.15	0.67	0.17
3	0.28	1.14	0.7	0.37
4	0.45	1.0	0.9	0.65

We looked at how consistent the exponents are for each given n. The exponents $\gamma/\nu_{\|\|}$ and $\beta/\nu_{\|\|}$ are obtained from the size dependence at $K_c \approx 0.342$. In Table I we list these *effective* exponents. In the fourth column we have $\nu_\perp/\nu_{\|\|}$, calculated from a hyperscaling relation. The last column gives the difference of the calculated value in the fourth column and the assumed value $1/n$. If the choice of n is correct, we should have zero in the last column. It is seen that none of the choices is very consistent.

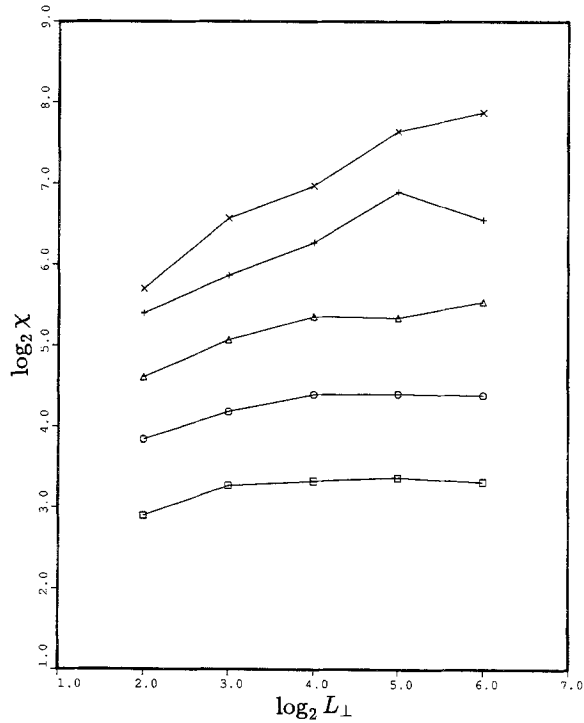

Fig. 19. Susceptibility at $K = 0.342$ of fully periodic finite systyems plotted against $L_\perp$ for given $L_{\|} = 2^n$, from bottom to top, where $n = 2, 3, 4, 5, 6$.

2.4.2. Scaling of Susceptibility and Magnetization. We carried out a finite-size analysis for the susceptibility and magnetization of periodic systems with sizes $2^n \times 2^m$, $n, m = 2, 3, 4, 5, 6$. The predictions of finite-size scaling[16] in this case are

$$\chi(T_c) \propto L_{||}^{\gamma/\nu_{||}}, \qquad \langle |\Psi| \rangle_{T_c} \propto L_{||}^{\gamma/2\nu_{||} - 1/2} L_{\perp}^{1/2}, \qquad L_{||} \ll L_{\perp}^{\nu_{||}/\nu_{\perp}} \tag{6}$$

$$\chi(T_c) \propto L_{\perp}^{\gamma/\nu_{\perp}}, \qquad \langle |\Psi| \rangle_{T_c} \propto L_{\perp}^{\gamma/2\nu_{\perp} - 1/2} L_{||}^{1/2}, \qquad L_{||} \ll L_{\perp}^{\nu_{||}/\nu_{\perp}} \tag{7}$$

Figures 19 and 20 are plots of the susceptibility and magnetization of those systems. Applying formula (6) to the data, we found $\gamma/\nu_{||} \approx 1.0$ from the susceptibility in the large-$L_{\perp}$ limit, where the susceptibility becomes independent of the dimension $L_{\perp}$. The growth of these saturation values with the size $L_{||}$ gives the exponent $\gamma/\nu_{||}$. This choice of $\gamma/\nu_{||}$ is fully consistent with the size dependence of the order parameter, where $\langle |\Psi| \rangle$ has no $L_{||}$ dependence and the trivial square-root dependent on $L_{\perp}$ is observed. This implies $2\beta/\nu_{||} \approx \nu_{\perp}/\nu_{||}$ from the hyperscaling relation. Using $\nu_{||} = 1$, $\beta = 0.22$, we then have $\nu_{\perp}/\nu_{||} = 0.44$. The other limiting behavior, $L_{||} \gg L_{\perp}^{\nu_{||}/\nu_{\perp}}$, is

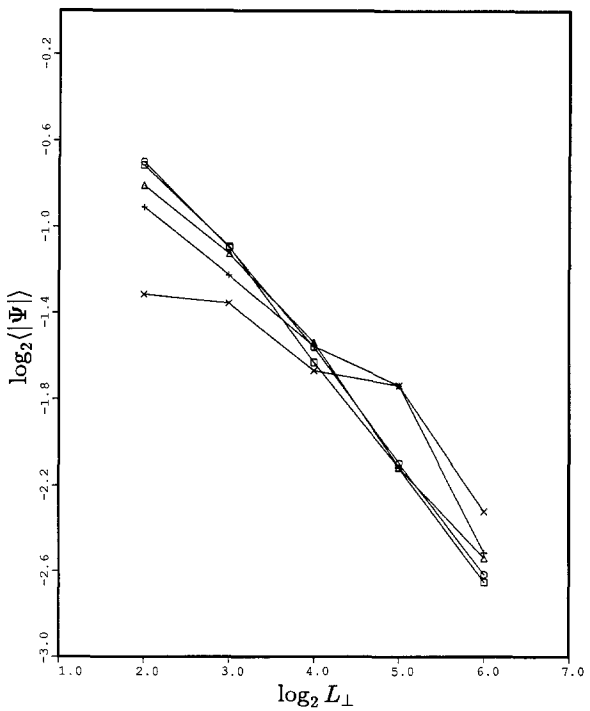

Fig. 20. Magnetization of fully periodic finite systems plotted against $L_{\perp}$ for given $L_{||}$ at $K = 0.342$. The sizes are the same as in Fig. 19.

difficult to obtain. Figures 21 and 22 are scaling plots with the above exponents: the quality of the data is not very good.

Apparently, there is a discrepancy between the subsystem result and the fully periodic one; cf. discussion in the last section.

2.5. Correlation Length of a Strip

The scaling theory[16] predicts that the correlation length at T_c of an infinitely long strip perpendicular to the field direction behaves as $\xi_\perp^0 \simeq a_\perp L_\parallel^{\nu_\perp/\nu_\parallel}$, and similarly $\xi_\parallel^0 \simeq a_\parallel L_\perp^{\nu_\parallel/\nu_\perp}$ for a strip along the field direction. The correlation function itself has to scale like

$$G_\perp(x) \simeq L_\parallel^{-\eta_\parallel^{RS}} \tilde{g}_\perp(x/\xi_\perp^0) \tag{8}$$

for a strip perpendicular to the field and

$$G_\parallel(z) \simeq L_\perp^{-\eta_\perp^{RS}} \tilde{g}_\parallel(z/\xi_\parallel^0) \tag{9}$$

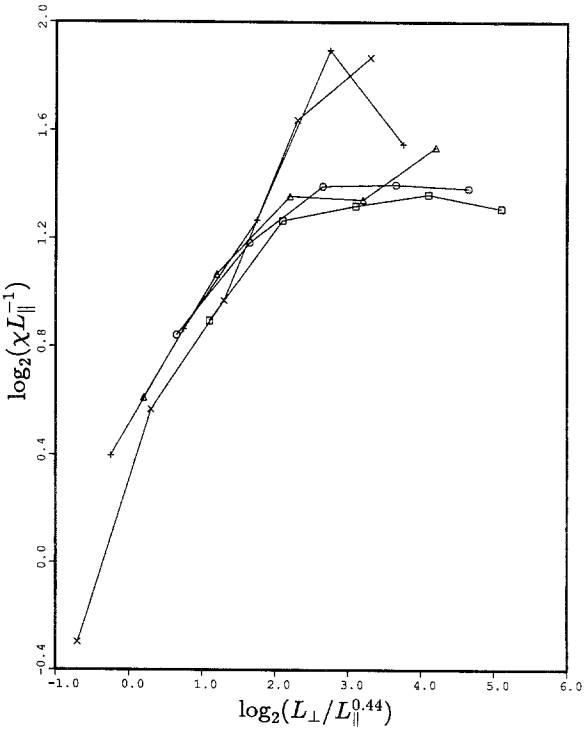

Fig. 21. Fully periodic system scaling plot $\chi L_\parallel^{-\gamma/\nu_\parallel}$ vs. $L_\perp/L_\parallel^{\nu_\perp/\nu_\parallel}$, with $\gamma/\nu_\parallel = 1$, $\nu_\perp/\nu_\parallel = 0.44$.

for the other orientation. The standard Ising model obeys these scaling forms.[17] In principle, such an analysis can given good estimates of the ratio of the ν and η exponents. If we allow $T \neq T_c$ data to go into the analysis, we can also find $\nu_{||}$ or $\nu_\perp$ individually.

For $p = 0.1$ the correlation length $\xi^0_{||}$ is very long. When $L_\perp = 4$, it is of order 60. Due to such long correlation lengths, we were unable to obtain reliable data. However, the method works better for the $p = 0$ case, which we shall discuss in the next section.

3. PURE DRIVEN KAWASAKI MODEL

The correlation functions for this system become negative at large distances due to particle number conservation. This effect is particularly severe for strips perpendicular to the field and makes it difficult to extract reliable information. Therefore we consider the strip geometry along the field only. The strong effect of the strip width can be seen from the fact that

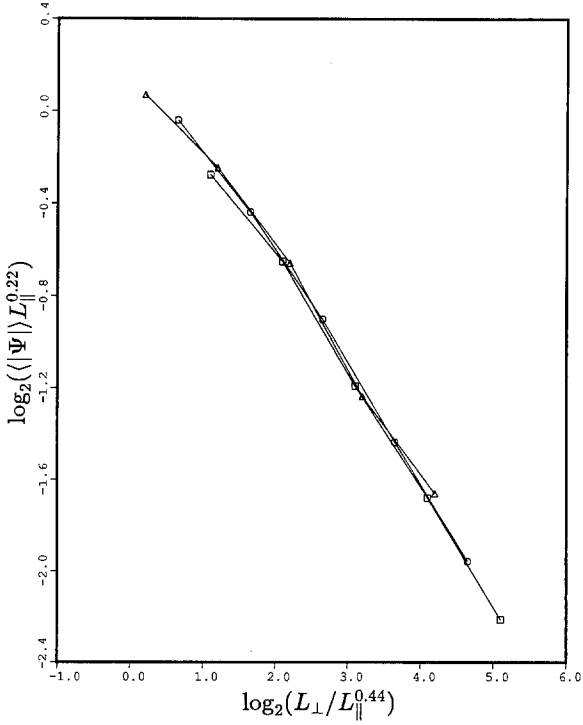

Fig. 22. Fully periodic subsystem scaling plot $\langle|\Psi|\rangle L_{||}^{\beta/\nu_{||}}$ vs. $L_\perp/L_{||}^{\nu_\perp/\nu_{||}}$. Here $\beta/\nu_{||} = 0.22$, $\nu_\perp/\nu_{||} = 0.44$.

for a strip with linear dimensions 256×3 the correlation function at $K = 0.325$, which corresponds to $K_c(p=0)$,[5] looks exponential with a decay length 1.2. This is in contrast to the $p = 0.1$ case, where for such a strip at $K_c(p=0.1)$ the correlation length is of order 50. Figure 23 is a plot of the correlation function $G_{||}(z)$ for $L_{||} = 256$ and $L_\perp = 6$, 10, 12, and 14. Good quality data are obtained. The correlation function clearly decays exponentially at large distances.

In Fig. 24 we plot the correlation length obtained from the slope in Fig. 23 vs. strip width $L_\perp$. In the same plot we also plot data for $K = 0.33$. For $L_\perp < 12$ the difference in temperature makes little difference in the correlation length. But the difference becomes big for larger sizes. On the other hand, the data for $L_\perp > 12$ are less reliable due to long correlation times and finite $L_{||}$. For $L_\perp = 20$ the correlation length ($\xi^0_{||} \approx 100$) is already comparable with the total system size ($L_{||} = 512$). Considering only $6 \leqslant L_\perp \leqslant 14$, we have from the slope $v_{||}/v_\perp \approx 2.24$. Assuming that the amplitude of the exponential decay goes with size as $L_\perp^{-\eta_\perp^{RS}}$, we deduce $\eta_\perp^{RS} \approx 1$. Figure 25 is a scaled plot with those exponents. Using $v_{||}\eta_{||}^{RS} =$

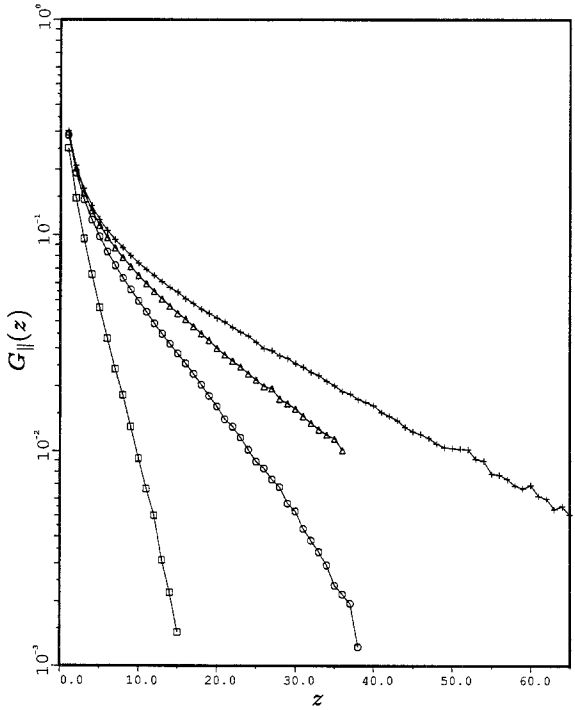

Fig. 23. Correlation function $G_{||}(z)$ for a strip parallel to the field. (□) $L_\perp = 6$, (○) $L_\perp = 10$, (△) $L_\perp = 12$, (×) $L_\perp = 14$. Longitudinal dimension $L_{||}$ is 256.

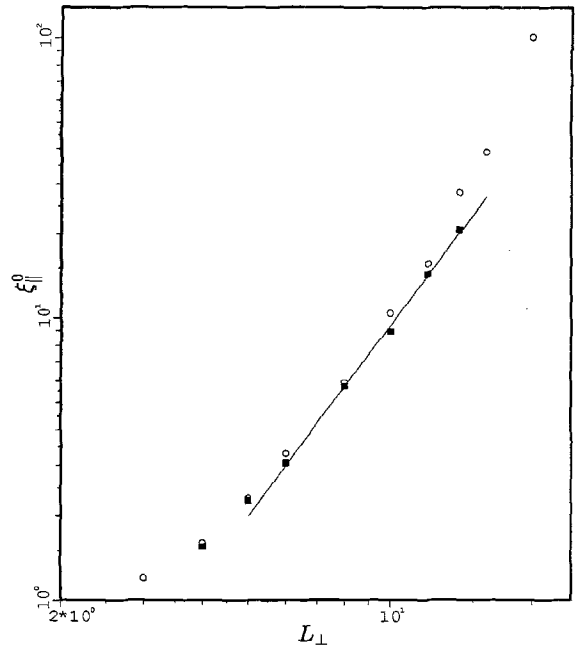

Fig. 24. Correlation length $\xi_{||}^0$, obtained from Fig. 23 by considering an exponential decay, vs. strip width $L_\perp$ in log–log scale. Squares are for $K=0.325$, circles are for $K=0.33$.

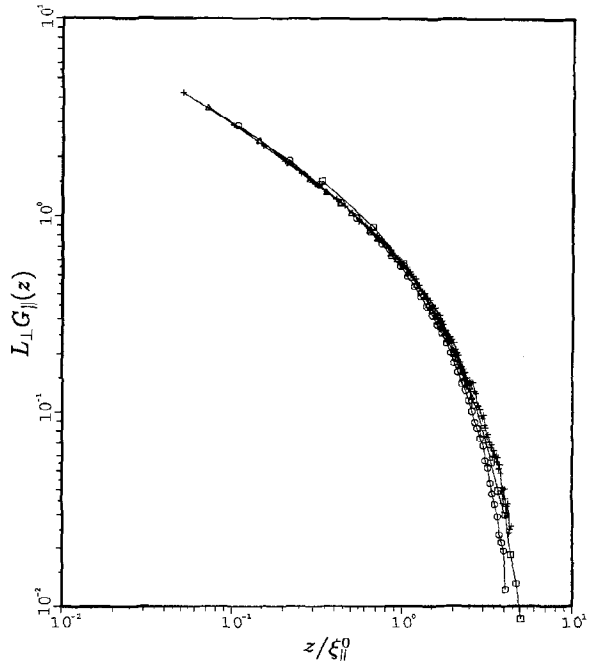

Fig. 25. Scaling plot $L_\perp G_{||}(z)$ vs. $z/\xi_{||}^0$.

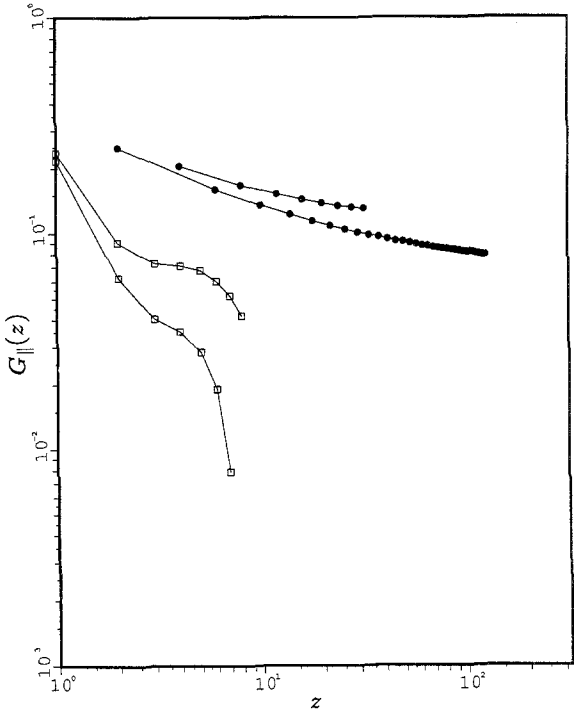

Fig. 26. Correlation functions of a system of size 256×64 (upper) and 512×64 (lower) for $p = 0$ at $K = 0.325$. (●) Longitudinal correlation, (□) transverse.

$\nu_\perp \eta_\perp^{RS}$, we have $\eta_{||}^{RS} \approx 0.45$. This is more or less consistent with direct calculation on large systems (128×64, 512×64) giving $\eta_{\downarrow|}^{RS} \approx 0.4$ (see Fig. 26). [For the transverse correlation only the first two data points ($x \leqslant 2$) seem reliable, so we cannot compute $\eta_\perp^{RS}$ directly.] However, a direct estimate from the slope in Fig. 25 gives $\eta_{||}^{RS} \approx 0.53$. A possible explanation is that the critical coupling K_c at $p = 0$ is not as accurately located as that for $p = 0.1$. This could alter the value $\nu_{||}/\nu_\perp$. Actually, we see from Fig. 26 that the longitudinal correlation curves are not at all straight lines, which indicates that the temperature is probably a bit too low.

4. SIMULATION RESULTS AT $p = 1/2$

The results of the previous sections indicate that the model with $p = 0.1$ already has isotropic critical exponents but very anisotropic amplitudes, and therefore is hard to analyze. This difficulty should be less serious for a larger value of p. We simulated the same model at $p = 1/2$.

From the 128×64 data, we have an estimate $K_c = 0.395$. We see again that the transverse and longitudinal η exponents are the same, $\eta_{||}^{RS} \approx 0.32$. The two-point correlations would be approximately isotropic if the distance in the longitudinal direction is normalized from z to $\rightarrow z' = 0.6z$, which is again close to pz as for the $p = 0.1$ case. For this reason we consider subsystems of block size ($L_{||}$, $L_\perp = L_{||}/2$) with $L_{||} = 8$, 16, 32, 64, 128. Using the result $\eta_{||}^{RS} = \eta_\perp^{RS}$, which implies $\nu_{||} = \nu_\perp = \nu$ from the scaling relation, we find $\gamma/\nu = 1.65$, $\beta/\nu = 0.16$. The set of exponents is close to but still different from the Ising exponents $\eta = 0.25$, $\gamma/\nu = 1.75$, $\beta/\nu = 0.125$. The exponents thus seem to depend in a continuous fashion on p: but it is quite possible that, due to crossover problems, we observe "effective exponents" only.

5. DISCUSSION

Our computer simulation study suggests: (1) for $p = 0.1$, $\nu_{||} \approx \nu_V = 1$, and $\eta_{||}^{RS} \approx \eta_\perp^{RS} \simeq 0.45$, $\beta \approx 0.22$ and $\gamma \simeq 1.55$. The anisotropy then lies in the amplitudes. (2) For $p = 0$, we have $\nu_{||} > \nu_\perp$, with the ratio probably close to 2. However, we consider our results for $p = 0$ inconclusive due to difficulties in bringing large systems to a stationary state.

As we have noted, the above behavior is not consistent with a scaling analysis of finite periodic systems. Such an analysis would lead us to believe that $\nu_{||} > \nu_\perp$ even for $p = 0.1$. In fact, the fourth moments discussed in Section 2.4.1 and the finite-size scaling in Section 2.4.2 are consistent with $\nu_{||}/\nu_\perp \approx 2$, but not with 1. This inconsistency is probably due to crossover effects which might introduce another length scale, controlled by p, such that for smaller lengths the system behaves essentially as it does at $p = 0$. More theoretical as well as computer work is clearly necessary for these systems.

APPENDIX A. CONSTRUCTION OF SUITABLE "ORDER PARAMETER COMPONENTS"

In this Appendix we wish to analyze finite-size effects near the phase transition to the ordered phase for systems where the global order parameter is conserved (typically it is fixed at zero, its value in the disordered phase of the system). Examples of such systems are the Kawasaki spin-exchange Ising problem[11] or its generalization where one applies an "electric field" E in one lattice direction, which has been called the z direction,[1–8] and of course also real fluids with a fixed particle number and volume.

Due to the constraint that the global order parameter is zero, the ordered state of the system is necessarily nonuniform. As discussed briefly

earlier,[20] the precise nature of this nonuniformity depends on the boundary conditions, as well as on the shape of the system.[21] Here we are interested in a d-dimensional hypercubic lattice with a linear dimension $L_{||}$ in the z direction and a linear dimension $L_\perp$ in the remaining $d-1$ lattice directions.

Figure 27 shows the expected ordered states for $d=2$, both for free and for periodic boundary conditions, and Fig. 28 the analogous situation for $d=3$. Note that we wish to consider situations where both $L_{||}$ and $L_\perp$ are much larger than the correlation length (or lengths, respectively, if the system is intrinsically anisotropic): then the domain configuration which must result from the principle that in thermal equilibrium the free energy is minimized is determined by the condition that the total interfacial free energy ("interfacial tension" times the interface area) is minimized, which means that the minimum number of interfaces occur consistent with the boundary conditions (i.e., one interface in the case of free boundary conditions, two interfaces for periodic boundary condition).

Although no such thermodynamic minimization principle exists for the far-from-equilibrium situation in the case where $E \neq 0$, we *assume as a working hypothesis* that the states characterizing the stationary probability distribution have a correspondingly minimized number of interfaces.

For the simple Ising problem on the square lattice with $E=0$ and uniform exchange interaction J, the solution will be provided by cases (a) and (b) if one has $L_{||} > L_\perp$ for the free boundary conditions, and (e) for periodic boundary conditions, while for $L_{||} < L_\perp$ cases (c), (d), or (f) will be the correct solution. While the free boundary condition breaks translational invariance and therefore the interface must occur (for zero total order parameter!) always midway in the system, the periodic boundary condition still maintains translational invariance: i.e., one interface coordinate (z_1 in the case of Fig. 27e, x_1 in the case of Fig. 27f) can be chosen freely; the coordinate of the second one then follows from the condition that the total order parameter is zero.

This extra translational degree of freedom for the interface position in the case of periodic boundary conditions has the consequence that it is easier to understand the free boundary case, and that is what we hence attempt to do first. We define transverse and longitudinal order parameters $\Psi_\perp$, $\Psi_{||}$ as follows (we consider only the case where $L_\perp$, $L_{||}$ are even integers, the lattice spacing being unity):

$$\Psi_\perp = \frac{1}{L_{||} L_\perp} \sum_{x=1}^{L_\perp} \left\{ \sum_{z=1}^{L_{||}/2} s(x,z) - \sum_{z=L_{||}/2+1}^{L_{||}} s(x,z) \right\} \tag{A.1}$$

$$\Psi_{||} = \frac{1}{L_{||} L_\perp} \sum_{z=1}^{L_{||}} \left\{ \sum_{x=1}^{L_\perp/2} s(x,z) - \sum_{x=L_\perp/2+1}^{L_\perp} s(x,z) \right\} \tag{A.2}$$

Note that the degeneracy between (a) and (b) [or (c) and (d), respectively] just means a sign change of the order parameters, and the order parameters are normalized to unity in a perfectly aligned configuration.

The equivalent definitions for a lattice of dimensionality $d=3$ are easily written down, observing (Fig. 28) that two parallel components $\Psi_{||}^{(1)}$, $\Psi_{||}^{(2)}$ need to be considered:

$$\Psi_{\perp}=\frac{1}{L_{||}L_{\perp}^{2}}\sum_{x=1}^{L_{\perp}}\sum_{y=1}^{L_{\perp}}\left\{\sum_{z=1}^{L_{||}/2}s(x,y,z)-\sum_{z=L_{||}/2+1}^{L_{||}}s(x,y,z)\right\} \tag{A.3}$$

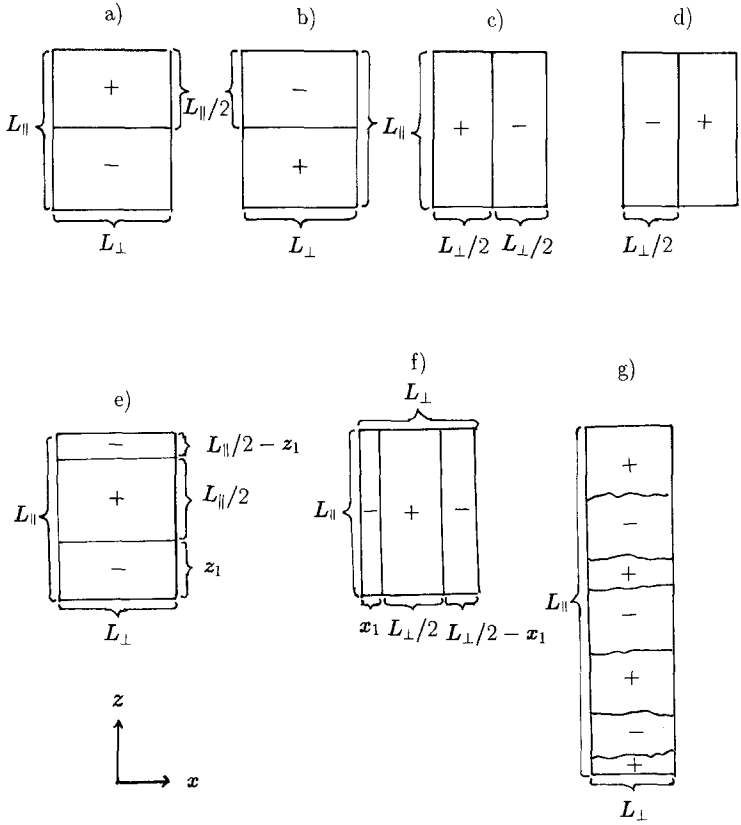

Fig. 27. Domain configurations of a two-dimensional Ising model below T_c, assuming a constraint that the total magnetization is zero, for free boundary conditions [case (a)–(d)] and periodic boundary conditions [(e), (f)] in a geometry $L_{\perp} \times L_{||}$. It is assumed that all lengths $L_{||}$, $L_{\perp}$ are much larger than the correlation length(s) of the system, and that the ratio $L_{||}/L_{\perp}$ neither approaches zero nor infinity, and thus multidomain-configurations [for example, case (g)] need not be considered. For more explanation, see text.

$$\Psi_{||}^{(1)} = \frac{1}{L_{||} L_\perp^2} \sum_{y=1}^{L_\perp} \sum_{z=1}^{L_{||}} \left\{ \sum_{x=1}^{L_\perp/2} s(x, y, z) - \sum_{x=L_\perp/2+1}^{L_\perp} s(x, y, z) \right\} \quad \text{(A.4)}$$

$$\Psi_{||}^{(2)} = \frac{1}{L_{||} L_\perp^2} \sum_{x=1}^{L_\perp} \sum_{z=1}^{L_{||}} \left\{ \sum_{y=1}^{L_\perp/2} s(x, y, z) - \sum_{y=L_\perp/2+1}^{L_\perp} s(x, y, z) \right\} \quad \text{(A.5)}$$

It is quite obvious how those definitions are generalized to a d-dimensional hypercubic geometry, with then $(d-1)$ order parameter "components" $\Psi_{||}^{(j)}$, in addition to one perpendicular component $\Psi_\perp$.

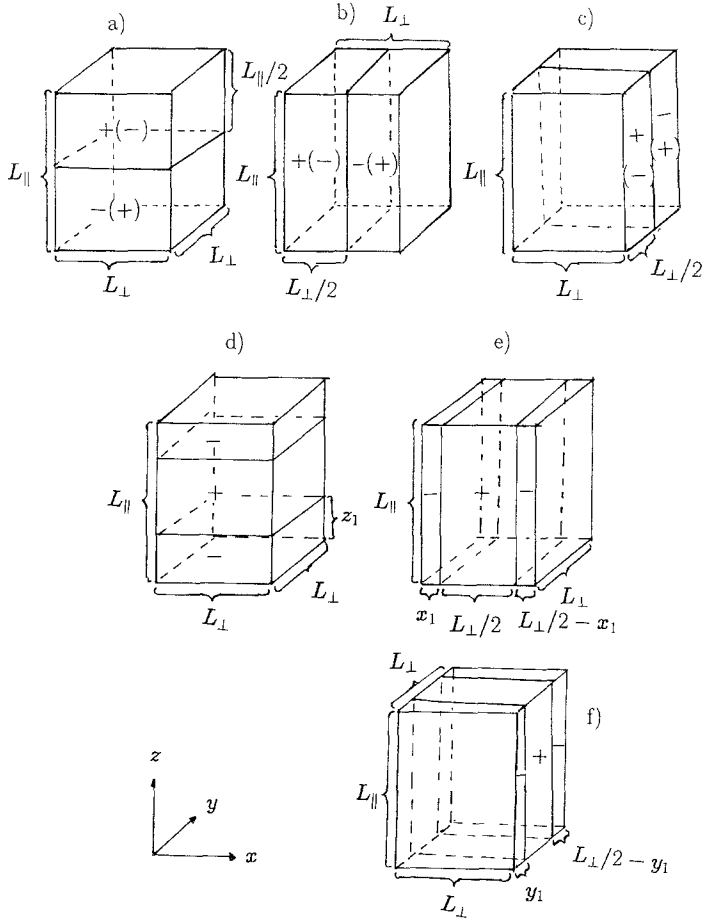

Fig. 28. Domain configuration of a three-dimensional Ising model below T_c, assuming a constraint that the total magnetization is zero, for free boundary conditions [case (a)–(c)] and periodic boundary conditions [(d)–(f)], in a geometry $L_\perp \times L_\perp \times L_{||}$. In the free boundary cases, two sign assignments for the magnetization in the domains are indicated. For further explanation see text.

It is conceivable to carry over these definitions to the periodic boundary case, but then the extra degree of freedom characterizing the interface position will show up explicitly. For example, for the two-dimensional case this would yield

$$\Psi_{\perp}(z_1)=\frac{1}{L_{||}L_{\perp}}\sum_{x=1}^{L_{\perp}}\left\{\sum_{z=z_1}^{z_1+L_{||}/2-1}s(x,z)-\sum_{z=z_1+L_{||}/2}^{z_1+L_{||}-1}s(x,z)\right\} \tag{A.6}$$

$$\Psi_{||}(x_1)=\frac{1}{L_{||}L_{\perp}}\sum_{z=1}^{L_{||}}\left\{\sum_{x=x_1}^{x_1+L_{\perp}/2-1}s(x,z)-\sum_{x=x_1+L_{\perp}/2}^{x_1+L_{\perp}-1}s(x,z)\right\} \tag{A.7}$$

where coordinates $z>L_{||}$, $x>L_{\perp}$ are reduced to $z-L_{||}$, $x-L_{\perp}$ by the periodic boundary condition. Similar equations could be written down for $d=3$ and periodic boundary condition as well.

However, since we ultimately are interested in an application of these concepts to numerical work (Monte Carlo or molecular dynamics calculations, if one considers continuum instead of lattice problems), we avoid considering order parameters such as Eqs. (A.6) and (A.7) which contain explicit information on the interface position. Instead of projecting the spin configuration with the Heaviside step function $1-2H(z-z_1)+2H(z-z_1-L_{||}/2)$, or $1-2H(x-x_1)+2H(x-x_1-L_{||}/2)$, with $H(z>0)=1$ while $H(z<0)=0$, which is the meaning of Eqs. (A.6)–(A.7), we project the spin configuration with $\sin\varphi$ and $\cos\varphi$ functions: although each of these harmonic functions is of course sensitive to the choice of a "phase" and hence to the interface position (z_1 or x_1), the property $\sin^2\varphi+\cos^2\varphi=1$ independent of φ means that out of the two components formed with $\sin\varphi$ and $\cos\varphi$ we can form a mean square order parameter for both the longitudinal and the transverse order parameters. For this purpose, the gauge of the phase is irrelevant, and hence we define (N is a normalization factor)

$$\Psi_{\perp}^{(\sin)}=\frac{N}{L_{||}L_{\perp}}\sum_{x=1}^{L_{\perp}}\sum_{z=1}^{L_{||}}s(x,z)\sin\left(\frac{2\pi}{L_{||}}z\right) \tag{A.8}$$

$$\Psi_{\perp}^{(\cos)}=\frac{N}{L_{||}L_{\perp}}\sum_{x=1}^{L_{\perp}}\sum_{z=1}^{L_{||}}s(x,z)\cos\left(\frac{2\pi}{L_{||}}z\right) \tag{A.9}$$

$$\Psi_{||}^{(\sin)}=\frac{N}{L_{||}L_{\perp}}\sum_{x=1}^{L_{\perp}}\sum_{z=1}^{L_{||}}s(x,z)\sin\left(\frac{2\pi}{L_{\perp}}x\right) \tag{A.10}$$

$$\Psi_{||}^{(\cos)}=\frac{N}{L_{||}L_{\perp}}\sum_{x=1}^{L_{\perp}}\sum_{z=1}^{L_{||}}s(x,z)\cos\left(\frac{2\pi}{L_{\perp}}x\right) \tag{A.11}$$

We determine the normalization factor N by considering the geometry of Fig. 27e) and a perfectly aligned spin configuration, where $s(x, z) = -1$, $1 \leqslant z < z_1$, and $z_1 + L_{||}/2 \leqslant z \leqslant L_{||}$, and $s(x, z) = +1$, otherwise. To find

$$\Psi_{||}^{(\sin)} = \frac{N}{L_{||}} \left\{ \sum_{z=z_1}^{z_1 + L_{||}/2 - 1} \sin\left(\frac{2\pi}{L_{||}} z\right) - \sum_{1}^{z_1} \sin\left(\frac{2\pi}{L_{||}} z\right) - \sum_{z_1 + L_{||}/2}^{L_{||}} \sin\left(\frac{2\pi}{L_{||}} z\right) \right\} \tag{A.12}$$

$$\Psi_{||}^{(\cos)} = \frac{N}{L_{||}} \left\{ \sum_{z=z_1}^{z_1 + L_{||}/2 - 1} \cos\left(\frac{2\pi}{L_{||}} z\right) - \sum_{1}^{z_1} \cos\left(\frac{2\pi}{L_{||}} z\right) - \sum_{z_1 + L_{||}/2}^{L_{||}} \cos\left(\frac{2\pi}{L_{||}} z\right) \right\} \tag{A.13}$$

Since we wish to consider $L_{||} \to \infty$, $L_{\perp} \to \infty$, in Eqs. (A.12) and (A.13) the sums may be converted to integrals:

$$\begin{aligned} \Psi_{||}^{(\sin)}(z_1) &= \frac{N}{L_{||}} \left\{ \int_{z_1}^{z_1 + L_{||}/2} \sin\left(\frac{2\pi}{L_{||}} z\right) dz \right. \\ &\quad \left. - \int_0^{z_1} \sin\left(\frac{2\pi}{L_{||}}\right) dz - \int_{z_1 + L_{||}/2}^{L_{||}} \sin\left(\frac{2\pi}{L_{||}} z\right) dz \right\} \\ &= 4 \frac{N}{2\pi} \cos\left(\frac{2\pi z_1}{L_{||}}\right) \end{aligned} \tag{A.14}$$

$$\begin{aligned} \Psi_{||}^{(\cos)} &= \frac{N}{L_{||}} \left\{ \int_{z_1}^{z_1 + L_{||}/2} \cos\left(\frac{2\pi}{L_{||}} z\right) dz \right. \\ &\quad \left. - \int_0^{z_1} \cos\left(\frac{2\pi}{L_{||}}\right) dz - \int_{z_1 + L_{||}/2}^{L_{||}} \cos\left(\frac{2\pi}{L_{||}} z\right) dz \right\} \\ &= 4 \frac{N}{2\pi} \sin\left(\frac{2\pi z_1}{L_{||}}\right) \end{aligned} \tag{A.15}$$

Thus we find

$$[\Psi_{||}^{(\sin)}(z_1)]^2 + [\Psi_{||}^{(\cos)}(z_1)]^2 = \frac{N^2}{(\pi/2)^2} \tag{A.16}$$

independent of z_1 and the linear dimensions, as desired. Normalizing the ordered state described above to a mean square order parameter of unity yields the normalization factor

$$N = \pi/2 \tag{A.17}$$

Considering instead of Fig. 27c the geometry of Fig. 27f, the calculation is identical, with z replaced by x and $L_{||}$ by $L_{\perp}$.

We now write down the definitions analogous to Eqs. (A.8)–(A.11) for higher dimensionality d,

$$\Psi_{\perp}^{(\sin)} = \frac{\pi/2}{L_{||} L_{\perp}^{d-1}} \sum_{x_1=1}^{L_\perp} \cdots \sum_{x_{d-1}=1}^{L_\perp} \sum_{z=1}^{L_{||}} s(x_1, \ldots, x_{d-1}, z) \sin\left(\frac{2\pi}{L_{||}} z\right) \tag{A.18}$$

$$\Psi_{\perp}^{(\cos)} = \frac{\pi/2}{L_{||} L_{\perp}^{d-1}} \sum_{x_1=1}^{L_\perp} \cdots \sum_{x_{d-1}=1}^{L_\perp} \sum_{z=1}^{L_{||}} (s(x_1, \ldots, x_{d-1}, z) \cos\left(\frac{2\pi}{L_{||}} z\right) \tag{A.19}$$

$$\Psi_{||}^{(\sin, j)} = \frac{\pi/2}{L_{||} L_{\perp}^{d-1}} \sum_{x_1=1}^{L_\perp} \cdots \sum_{x_{d-1}=1}^{L_\perp} \sum_{z=1}^{L_{||}} s(x_1, \ldots, x_{d-1}, z) \sin\left(\frac{2\pi}{L_\perp} x_j\right), \quad j = 1, \ldots, d-1 \tag{A.20}$$

$$\Psi_{||}^{(\cos, j)} = \frac{\pi/2}{L_{||} L_{\perp}^{d-1}} \sum_{x_1=1}^{L_\perp} \cdots \sum_{x_{d-1}=1}^{L_\perp} \sum_{z=1}^{L_{||}} s(x_1, \ldots, x_{d-1}, z) \cos\left(\frac{2\pi}{L_\perp} x_j\right), \quad j = 1, \ldots, d-1 \tag{A.21}$$

In summary of this section, we propose to use as "order parameter components" all possible Fourier transforms of the spin field with the smallest possible wavevectors, which are oriented in the various lattice directions. For an isotropic Ising model without electric field, i.e., the ordinary Kawasaki spin exchange Ising model, all these "components" obviously are equivalent, and the quantity to consider is simply

$$\Psi^2 = \Psi_{\perp}^2 + \sum_{j=1}^{d-1} \Psi_{||}^2(j) \tag{A.22}$$

$$\Psi_{||}^2(j) = [\Psi_{||}^{(\sin, z)}]^2 + [\Psi_{||}^{(\cos, z)}]^2 \tag{A.23}$$

In the case with electric field, however, components $\Psi_{\perp}^2$ and $\Psi_{||}^2$ are no longer equivalent; only the components $\Psi_{||}^2(j)$ are relevant; then all these components are of course equivalent, and hence we shall consider

$$\Psi_{||}^2 = \sum_{j=1}^{d-1} \Psi_{||}^2(j) \tag{A.24}$$

If we consider the average value $\langle \Psi^2 \rangle_T$, we can see directly from the definition, Eq. (A.18), that [denoting by $s(\mathbf{k}_\nu)$ the complex Fourier transform of the spin field $s(\mathbf{x})$]

$$\langle \Psi^2 \rangle_T \propto \sum_{\nu=1}^{d} \langle s(-\mathbf{k}_\nu)\, s(\mathbf{k}_\nu) \rangle_T / (L_{||} L_{\perp}^{d-1}) = \sum_{\nu=1}^{d} S(\mathbf{k}_\nu)/(L_{||} L_{\perp}^{d-1}) \tag{A.25}$$

with $\mathbf{k}_\nu$ being the wavevectors $(2\pi/L_{||})(1, \ldots, 0, 0)$, $(2\pi/L_{||})(0, 1, \ldots, 0), \ldots,$ $(2\pi/L_{||}(0, \ldots, 0, 1)$. For $T > T_c$ (and no electric field) this correlation func-

tion is just the static susceptibility $k_B T\chi$, apart from corrections of order $(k_v\xi)^2$ which are negligible for large enough $L_{||}$, $L_\perp$. Below T_c, it also is completely clear that $\langle \Psi^2 \rangle$ basically is proportional to the square of the spontaneous magnetization in the Ising model.

For the case including the electric field the contribution due to $\Psi_\perp$ is nonordering and hence should be omitted, which means we have to omit $\mathbf{k}_d$ from Eq. (A.25) [$\mathbf{k}_d = (2\pi/L_\perp)(0,..., 0, 1)$, $S(\mathbf{k})$ is the standard "structure factor"],

$$\langle \Psi^2 \rangle_T \propto S(\mathbf{k}_v)/(L_{||} L_\perp^{d-1}) \tag{A.26}$$

Qualitative evidence consistent with this description can be found in Figs. 4 and 7 of ref. 3, where for $d=2$ Eq. (A.26) was obtained for $L = L_{||} = L_\perp = 30$, as well as a different measure for the order parameter ("comparing the difference between the average of the magnetization squared in the vertical columns and horizontal rows and dividing the result by L^2").

In Monte Carlo simulations of $\langle \Psi^2 \rangle_T$, care must be taken at $T < T_c$ that nonequilibrium results (due to multidomain configurations) are avoided. This can be done, for instance, by starting the system initially in a perfectly aligned configuration of the type shown in Fig. 27f or Fig. 28e, respectively, which then is relaxed while "equilibrium" is achieved.

APPENDIX B. "LOCAL" VERSUS GLOBAL ORDER PARAMETERS

In previous work (e.g., ref. 3) a different "order parameter" was suggested, namely

$$\Delta\rho = (M_v^2 - M_h^2)^{1/2} \tag{B.1}$$

where "vertical" and "horizontal" magnetizations M_v and M_h are defined in terms of the local magnetization $m(x, y, z)$ of each site x, y, z of a three-dimensional lattice via

$$M_v^2 = \frac{1}{L_\perp^2} \sum_{x,y=1}^{L_\perp} \left[\frac{1}{L_{||}} \sum_{z=1}^{L_{||}} m(x, y, z) \right]^2 \tag{B.2}$$

$$M_h^2 = \frac{1}{L_{||}} \sum_{z=1}^{L_{||}} \left[\frac{1}{L_\perp^2} \sum_{x,y=1}^{L_\perp} m(x, y, z) \right]^2 \tag{B.3}$$

Why did we spend the effort in going through the discussion of Appendix A in constructing the description in terms of "order parameter components" instead of simply using Eqs. (B.2) and (B.3)?

The answer to this question is that Eq. (B.1) is in a sense a "local" order parameter only, measuring the order parameter difference between domains in any kind of "strip" domain arrangement (i.e., domains running through the system in the z direction), but is completely insensitive to the size and arrangement of these strip domains.

To show this assertion, we define an idealized strip domain structure via

$$m(x, y, z) = m_0 f(x, y) \tag{B.4}$$

where m_0 is the absolute value of the magnetization inside the domains and the function $f(x, y)$ describes the sign of the magnetization

$$f(x, y) = \pm 1, \qquad \sum_{x, y} f(x, y) = 0 \tag{B.5}$$

The second condition results from requiring that there is no average magnetization; which sign at site (x, y) actually is realized depends on the particular choice of strip configuration. Using Eqs. (B.4) and (B.5), it is trivial to show that

$$M_h^2 = 0, \qquad M_v^2 = m_0^2, \qquad \Delta\rho = m_0 \tag{B.6}$$

irrespective of the value of $f(x, y)$. Thus, $\Delta\rho$ measures the local order parameter inside a strip; it is independent of the width of the strips. In the standard Kawasaki model, this would correspond to measuring the local order parameter inside the (on average spherical) domains.

ACKNOWLEDGMENTS

Part of the computation was performed at the John von Neumann National Supercomputer Center. This work was supported in part by NSF grant DMR86-12369. Partial support of J.-S.W. was provided by a Supercomputer Fellowship. K.B. was supported in part by the Visiting Supercomputer Senior Scientist Program at Rutgers University.

REFERENCES

1. S. Katz, J. L. Lebowitz, and H. Spohn, *Phys. Rev. B* **28**:1655 (1983).
2. S. Katz, J. L. Lebowitz, and H. Spohn, *J. Stat. Phys.* **34**:497 (1984).
3. J. Marro, J. L. Lebowitz, H. Spohn, and M. H. Kalos, *J. Stat. Phys.* **38**:725 (1984).

4. J. L. Vallés and J. Marro, *J. Stat. Phys.* **43**:441 (1986).
5. J. L. Vallés and J. Marro, *J. Stat. Phys.* **49**:89 (1987).
6. J. Marro and J. L. Vallés, *J. Stat. Phys.* **49**:121 (1987).
7. J. Marro, J. L. Vallés, and J. M. González-Miranda, *Phys. Rev. B* **35**:3372 (1987).
8. M. Q. Zhang, Ph.D. Thesis, Rutgers University, New Brunswick, New Jersey (1987), unpublished.
9. M. Q. Zhang, J.-S. Wang, J. L. Lebowitz, and J. L. Vallés, *J. Stat. Phys.* **52**:1461 (1988).
10. R. Dickman, Preprint (1988).
11. K. Kawasaki, in *Phase Transitions and Critical Phenomena*, Vol. II, C. Domb and M. S. Green, eds. (Academic Press, New York, 1972), p. 443.
12. H. K. Janssen and B. Schmittmann, *Z. Physik B* **64**:503 (1986).
13. K.-T. Leung and J. Cardy, *J. Stat. Phys.* **44**:567 (1986).
14. R. J. Glauber, *J. Math. Phys.* **4**:294 (1963).
15. J.-S. Wang and J. L. Lebowitz, *J. Stat. Phys.* **51**:893 (1988).
16. K. Binder and J.-S. Wang, *J. Stat. Phys.* **55**:87 (1989).
17. J. L. Cardy, in *Phase Transitions and Critical Phenomena*, Vol. 11, C. Domb and J. L. Lebowitz, eds. (Academic Press, New York, 1987), p. 55.
18. P. L. Garrido and L. J. Lebowitz, Personal communication.
19. R. Zia, Personal communication.
20. K. Binder, *Z. Physik* **43**:119 (1981).
21. V. Privman and M. E. Fisher, *J. Stat. Phys.* **33**:385 (1983).